J Mater Sci (2014) 49:7585–7596
DOI 10.1007/s10853-014-8467-x

Carbon dioxide adsorption using amine-functionalized mesocellular siliceous foams

Juanjuan Ma · Qiming Liu · Dandan Chen · Yuan Zhou · Sheng Wen

Received: 19 May 2014 / Accepted: 11 July 2014 / Published online: 30 July 2014

Abstract Mesocellular siliceous foams (MCFs) with and without remaining template were prepared and modified by polyethylenimine (PEI) or mixed amines [Diethylenetriamine and PEI or 3-aminopropyltrimethoxysilane (APTMS) and PEI]. These samples were evaluated for their adsorption capacities for CO_2 at different temperatures. With the increase of PEI loading, the optimal adsorption temperature shifts to higher temperature for samples prepared in our study. The remaining template in MCF materials plays an important role in promoting CO_2 adsorption capacity, which could be 3.24 mmol/g when the amount of PEI loading is 70 % at 85 °C. Meanwhile, the remaining template contributes greatly to the dispersion of PEI, resulting in higher adsorption capacity at low temperature. The effect of the amount of remaining template was studied, and it was found that CO_2 adsorption capacity decreases with increasing template. The CO_2 adsorption capacities for mixed-amine-modified MCFs are higher than those of the samples modified by PEI only, which was ascribed to the better dispersion of PEI. MCF modified with the mixing of APTMS and PEI exhibited highest adsorption capacity of 2.67 mmol/g at 50 °C. These findings reveal that pore structure, PEI loading, PEI dispersion, and remaining template work together to influence the CO_2 adsorption performance.

J. Ma · Q. Liu (✉)
State Key Laboratory of Silicate Materials for Architectures, Wuhan University of Technology, Wuhan 430070, China
e-mail: qmliu@whu.edu.cn

Q. Liu · D. Chen · Y. Zhou
School of Physics and Technology, Key Laboratory of Artificial Micro- and Nano-structures of Ministry of Education, Wuhan University, Wuhan 430072, China

Q. Liu · S. Wen
College of Chemistry and Materials Science, Hubei Engineering University, Xiaogan 432000, China

Introduction

The increasing CO_2 concentration in the atmosphere has been regarded as a leading contributor to climate change in recent decades, and CO_2 capture and sequestration (CCS) has attracted considerable attention in the world. It has been reported that CO_2 concentration in the atmosphere has increased from about 310 ppm to over 380 ppm during the last half century [1]. CCS is currently a very active research area, which provides a mid-term solution allowing humanity to continue using fossil energy until renewable energy technologies mature. Before sequestration, CO_2 must be separated from flue gas, natural gas, or even air. The process of separation is obtained by physisorption and chemisorption between certain adsorbents and CO_2 molecules. Absorption by amine-based aqueous solution is currently one of the commercially available technologies for CO_2 separation. However, this process has major drawbacks, such as an energy-intensive regeneration step, oxidative degradation of the aqueous amines, and the corrosion of equipment [1]. In the past decade, development of processes based on solid adsorbents has been considered as alternative separation technologies for post-combustion CO_2 capture. Porous solids such as zeolites [2–5], activated carbons [6–9], hydrotalcites [10–14], metal–organic frameworks [15–17] and mesoporous silicas [18–32] are good candidates for capturing CO_2.

Apart from research efforts focusing on porous material, loading amines on porous materials also appear as a promising strategy for sorbent design and CO_2 separation/capture. There are two main ways to immobilize amines in

a porous material: grafting and impregnation. Grafting method, based on the chemical reaction between surface silanol groups and organosiloxane molecules, has been employed to incorporate aminated organosilanes into a wide range of silica porous supports. Organosilanes, such as 3-aminopropyltrimethoxysilane (APTMS) [33–38], *N*-(2-aminoethyl)-3-aminopropyltrimethoxysilane [39–42], and diethylenetriamino-trimethoxysilane [39, 40, 43, 44], have been grafted on different mesoporous silicas and evaluated their adsorption capacities toward CO_2. The influence of amine structure [39, 40, 44], pore structure [45, 46], amine surface density [47], stability and adsorption mechanism [34, 48–50] were studied. When the grafting method is used, CO_2 adsorption capacity depends on the amine density and the total nitrogen content. The total nitrogen content incorporated into the support is restricted by the amount of silanol groups present in the surface of porous structure and the number of amino groups that organosilane contains.

In order to incorporate a higher quantity of amino groups, increased attention has been paid to amine-modified adsorbents by impregnation for simple preparation and high adsorption capacity. Various mesoporous solid supports with different pore structures were investigated, such as SBA-15 [18–23], SBA-16 [24], SBA-12, MCM-41 [22–24, 31], MCM-48 [51], KIT-6 [24], MSU-1 [52], HMS [32], silica gel [53, 54], and mesocellular silica foam [25–29, 55, 56]. A series of studies had reported that the adsorbents with large total pore volume and pore diameter reached significant CO_2 uptakes, which is attributed to the positive effect of the large pore volume and pore diameter [19, 21, 23, 24]. Sayari and coauthors [22] showed the effect of pore length on CO_2 adsorption over amine-modified mesoporous silicas by impregnation. They reported that CO_2 adsorption performance was strongly dependent upon the pore length, and the materials with the shortest channels showed the highest capacity and fastest adsorption. Among all these factors, such as pore size, pore volume, pore length, and surface area, the importance of pore volume of the supports on CO_2 adsorption capacity was demonstrated. Mesocellular siliceous foam (MCF) with large pore size and high pore volume seems to be a suitable candidate for high-capacity CO_2 adsorbents.

In addition to focusing on the synthesis of different solid supports, efforts have also been made to the better dispersion of the amines (PEI or TEPA) in these supports. The influence of remaining template was studied and they reported that the remaining P123 template (P123 or CTAB) in the MCF played a great role in promoting the CO_2 adsorption capacity [26, 57–59]. Sayari and coauthors [31] reported that the layer of surface alkyl chains played an important role in enhancing the dispersion of PEI, thus decreasing the diffusion resistance. Wang et al. [52] concluded that TEPA was better distributed with the help of the template [alcohol polyoxyethylene ether (A (EO) 9)]. Ling and coauthors [60] utilized nine surfactants as promoters to facilitate the CO_2 diffusion from the surface into the bulk of PEI. As a result, nonionic surfactant sorbitan monooleate (Span80) was found to be an optimal candidate to promote CO_2 diffusion process. In a summary,the template remaining in the porous structure is favorable for the well distribution of the amine and CO_2 diffusion. However, the amount of remaining template has been studied rarely. Yan et al. investigated the support with remaining template partially removed by ethanol, and they concluded that CO_2 uptake increased with remaining template. In our preparation of mesoporous silicas, we found that the amount of remaining template differed with the amount of washing water when no other solvent was used. The pore diameter and pore volume decrease with remaining template, resulting in lower amine loading, which would decrease the CO_2 adsorption capacity. Though the remaining template plays an important role in CO_2 uptake, it is difficult to determine which contributes more. So in this paper, we investigated the influence of the amount of remaining template to CO_2 uptake. Except for the utilization of templates, mixed amines are also investigated to improve CO_2 adsorption performance [57, 61]. We also studied the effect of mixed amines to CO_2 adsorption capacity and amine efficiency, considering that the mixed amine could also contribute to the dispersion of macromolecule amines, such as PEI.

In this study, we synthesized MCF with the help of heptanes. Sun et al. [62] synthesized highly ordered large-pore SBA-15 with the help of alkanes and ammonium fluoride (NH_4F) at low temperature. According to their opinion, large-pore MCF would be synthesized at similar condition, except for higher initial reaction temperature. In our study, we chose heptanes to synthesize MCF for appropriate synthesis temperature and large pore volume.

Experimental

Chemicals/reagents

The materials used in experiment were as follows: Pluronic P123 EO–PO–EO triblock copolymer (Aldrich, Mw = 5800), heptanes (C_7H_{16}), tetraethyl orthosilicate (TEOS), hydrochloric acid (HCl), NH_4F, polyethyleneimine (PEI, Aldrich, Mn = 10000), methanol (CH_3OH), Diethylenetriamine (DETA), and APTMS.

Preparation of adsorbents

The MCF material was synthesized based on the procedure reported by Sun et al. [62]. 8 g P123 and 0.09 g NH_4F were

dissolved in 280 ml of HCl aqueous solution with a concentration of 1.3 M at room temperature. Then a solution of 49.93 ml heptanes and 16.75 ml TEOS was poured into under stirring. After stirring at 52 °C for 20 h, the resulting mixture was transferred into an autoclave and kept at 100 °C for 72 h. The mixture was cooled, filtered, washed with water, and dried at 60 °C for 24 h. Then the white solid was calcined at 550 °C for 6 h to remove the template, which was denoted as MCF(c). Template-remaining MCFs were also prepared to investigate the contribution of template to CO_2 adsorption capacity. MCF(a) was synthesized by following the same procedure, which was not washed by water. Water-washed sample MCF(w_1), MCF(w_2), and MCF(w_3) were also prepared by washing with different amount of water, respectively.

PEI-modified MCF was prepared by impregnation. Typically, a calculated amount of PEI was dissolved in CH_3OH under stirring for 30 min. Then a calculated amount of MCF powder was added into the solution. After being stirred until CH_3OH was volatilized, the mixture was dried at 60 °C for 12 h. The prepared amine-modified MCFs were denoted as MCF(c, a, w_1, w_2, w_3)/PEI−x, where x presents the weight percent of PEI in the material.

PEI (0.5 g) and DETA (0.2 g)/APTMS (0.2 g)/heptanes (0.1 g) were dissolved in CH_3OH (10 ml) under stirring for 30 min, and then 0.3 g MCF power was added into the solution. After being stirred until CH_3OH was volatilized, the mixture was dried at 60 °C for 12 h. The prepared mixed-amine-modified MCFs were denoted as MCF(c)/PEI + DETA, MCF(c)/PEI + APTMS, and MCF(c)/PEI + Hep, respectively.

Characterization

The adsorption–desorption isotherms of nitrogen at 77 K were obtained using a Micromeritics ASAP 2020 instrument. MCF samples were degassed at 120 °C for 120 min. While for amine-modified samples, they were degassed at 100 °C for 120 min. The Brunauer–Emmett–Teller (BET) surface area was calculated using the N_2 adsorption isotherm data within the relative pressure from 0.05 to 0.35. The pore volume was obtained at a relative pressure of 0.99. The pore size distributions were derived from the adsorption–desorption branch using the Barrett–Joyner–Halenda (BJH) model. The amounts of template remaining in the support washed by different amount of water were measured by a thermal gravimetric analysis (TGA, NETZSCH STA 449C). The sample was heated at 10 °C/min to 700 °C under N_2 flow (50 ml/min).

CO_2 adsorption measurements

The evaluation of CO_2 adsorption was performed in a fixed-bed reactor connected with a gas chromatography (GC), which is equipped with a thermal conductivity detector. The gas flow rate was controlled by a mass flow controller, and the adsorption temperature was controlled by a temperature-programmable furnace. All the measurements were conducted under atmospheric pressure. As the concentration in flue gas is about 10 %, a model gas containing 9.64 % CO_2 was chosen in the analysis. The diagram of the fixed-bed flow system is shown in Fig. 1.

In an adsorption process, about 0.5 g of the adsorbent was packed into the stainless steel column in the middle of the reactor supported with glass wool. Before each adsorption test, the adsorbent was pretreated at 100 °C for 2 h in H_2 stream at a flow rate of 30 ml/min to remove moisture and air. Then the adsorbent was cooled down to a desired temperature, and a model gas containing 9.64 % CO_2 and 90.36 % H_2 was introduced at a flow rate of 30 ml/min. The concentrations of CO_2 in the influent and effluent gas streams were monitored by the GC. The CO_2 adsorption capacity was calculated on the basis of breakthrough curves.

Results and discussion

Adsorbent characterization

The N_2 adsorption–desorption isotherms at 77 K and adsorption pore size (cell diameter) distribution curves for MCF(c) before and after PEI loading are shown in Fig. 2a. In the N_2 adsorption–desorption isotherms, MCF(c) displays a typical type IV adsorption isotherm with a clear capillary condensation at around $P/P_0 = 0.9$ along with a hysteresis loop, which indicates its uniform meso-structure and large pore size. The TEM and SEM of MCF(c) are shown in Fig. 2b and it can be seen a pore structure like foam. The determined BET surface area is 557.32 m^2/g and total pore volume is 2.38 cm^3/g. The pore with cell diameter of 20.46 nm and window diameter of 16.52 nm was obtained, indicating a pore shape similar like cylinder. In our previous experiment, mesoporous silica SBA-15 was synthesized without heptanes at 40 °C, and a total pore volume of 1.02 cm^3/g and a pore diameter of 7.60 nm were obtained (not shown). After PEI loading, the hysteresis loop can still be observed with 30 % PEI loading. When the loading amount continued to increase, no hysteresis loop can be obtained. The structural characteristics of a series of samples prepared in this work are summarized in Table 1. After PEI loading, the surface area and pore volume decrease greatly with increasing PEI loading. However, the pore diameter increased with PEI loading, which implied that part of PEI dominated onto the surface of the porous structure, resulting in aggregates. Considering that the density of PEI is about 1.00 g/cm^3, the

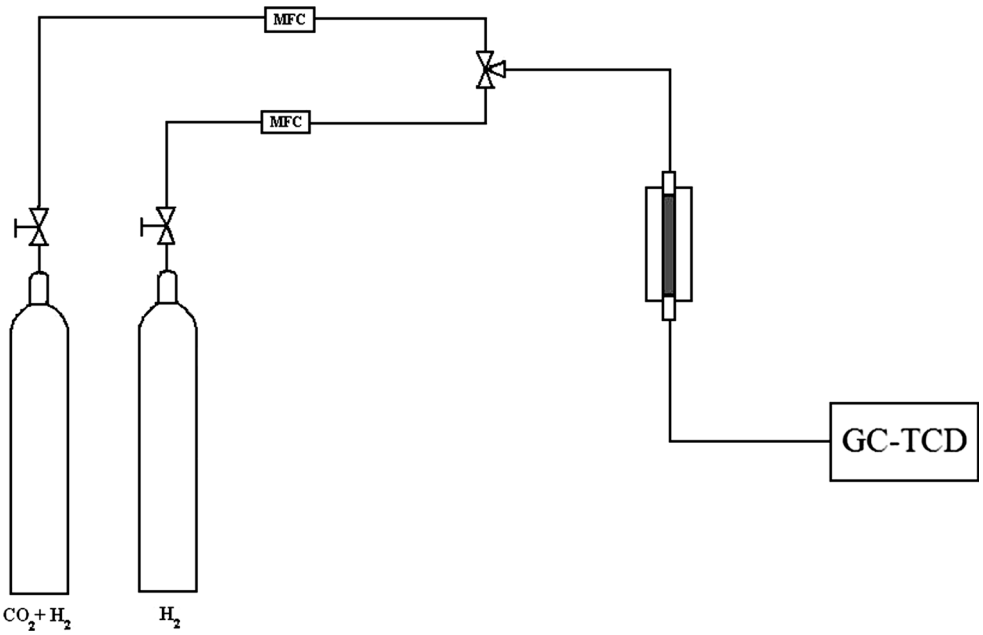

Fig. 1 The diagram of the fixed-bed flow system

theoretical maximum amount in MCF(c) is 70.41 wt%. Thus, for MCF(c)/PEI-30 and MCF(c)/PEI-50, the pore volume should be larger than the value obtained from adsorption–desorption isotherms. This implies that PEI firstly dominates the pore opening, which makes nitrogen molecules difficult to enter into the pores at 77 K. The SEM image of MCF(c)/PEI-30, as shown in Fig. 2b, reveals that PEI has been impregnated into MCF(c), resulting in the particles which began to aggregate. Further increasing the PEI loading to 70 %, the aggregation became serious. The phenomenon of aggregation was consistent with the result of N_2 adsorption–desorption isotherms, shown in Fig. 2a.

Figure 3 shows the nitrogen adsorption–desorption isotherms of MCF(c), MCF(a), MCF(w_1), MCF(w_2), and MCF(w_3) at 77 k and the corresponding adsorption pore size (cell diameter) distribution curves. Table 1 presents a summary of the corresponding textural properties of surface area, pore volume, cell diameter, and window diameter. Typical type IV adsorption isotherms with a H1 hysteresis loop are obtained for MCF(c), MCF(w_3), and MCF(w_2). MCF(w_3) and MCF(w_2) exhibit pore volume of 1.45 and 1.29 cm^3/g, respectively. However, for samples MCF(w_1) and MCF(a), the hysteresis loops are much smaller and the pore volumes are 0.84 and 0.39 cm^3/g, respectively. The pore volume decreases in the order of MCF(c) > MCF(w_3) > MCF(w_2) > MCF(w_1) > MCF(a). The surface area exhibits a similar trend as the pore volume. This may give a clue that the amount of remaining template is different in these samples. Figure 4a shows the TGA profiles of MCF(c), MCF(a), MCF(w_1), MCF(w_2), and MCF(w_3), and the accompanying differential thermal gravimetric analysis (DTGA) results are also included in Fig. 4b. As shown, MCF(c) lost 3.61 % of its original mass before 100 °C, which can be mainly ascribed to desorption of CO_2 and moisture. MCF(a) show two weight losses, with a large loss from 300 to 500 °C. It can be seen from Fig. 4b that two sharp weight losses occur at 110 and 370 °C, indicating the decomposition of heptanes and P123. The other three samples washed by different amount of water all exhibit one sharp weight loss between 300 and 400 °C, which can be ascribed to the decomposition of P123. Except for moisture and CO_2, the weight loss of MCF(a), MCF(w_1), MCF(w_2), and MCF(w_3) is 53.88, 47.58, 36.36, and 35.18 %, respectively, which is consistent with the pore volume of these four samples. It can be concluded that the amount of remaining template is different in the support washed with different amount of water.

CO_2 adsorption performance of MCF(c)

CO_2 adsorption characteristics of MCF(c) with 30, 50, 70, and 80 % PEI loading were investigated at 30, 50, 75, and 100 °C under a gas containing 9.64 % CO_2 at a flow rate of 30 ml/min in a fixed-bed flow system. The breakthrough curves of MCF(c)/PEI-70 at different temperatures are shown in Fig. 5a. It can be seen that most of the adsorption capacity was obtained before breakthrough. And the outlet CO_2 concentration reached breakthrough quickly at 30, 50, and 75 °C. While the breakthrough curve at 100 °C was an exceptional situation, the outlet CO_2 concentration reached breakthrough more slowly. The same phenomenon occurred for other three samples at 100 °C. The surface area of

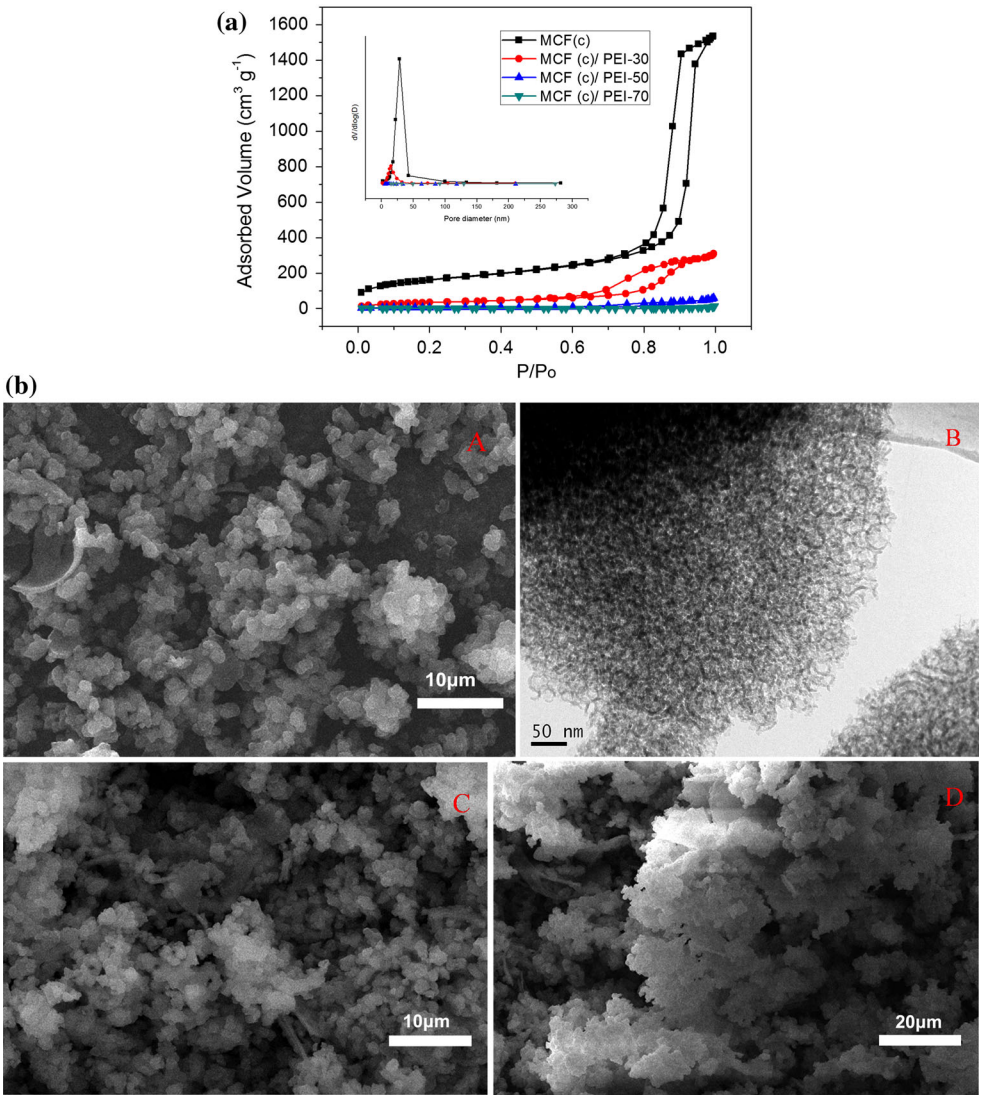

Fig. 2 **a** Nitrogen adsorption–desorption isotherms at 77 K for MCF(c) before and after PEI loading. **b** SEM images of *A*. MCF(c), *C*. MCF(c)/PEI-30, *D*. MCF(c)/PEI-70, and TEM images of *B*. MCF(c)

MCF(c)/PEI-70 is very low (1.14 cm^2/g), suggesting that chemisorption contributes to most of the adsorption capacity. As we know, adsorption is an exothermal process, and the adsorption of CO_2 becomes thermodynamically unfavorable at higher temperature, resulting in slow adsorption rate before breakthrough at 100 °C. At 50 min, the effluent CO_2 concentrations of MCF(c)/PEI-70 at 30, 50, 70, and 100 °C were 9.6038, 9.5524, 9.5102, and 9.7029 %, respectively. The outlet concentration at 100 °C even was higher than the model concentration, which can be ascribed to the desorption rate that was faster than adsorption rate at high temperature. At 100 °C, the adsorbent reached saturation in 20 min, while it did not reach saturation even in 1 h at 30, 50, and 75 °C. Song and coauthors [63] conducted an infrared study on PEI-modified SBA-15, and they confirmed that the molecular flexibility of PEI increased with temperature, which contributed to the increase of CO_2 adsorption capacity at high temperature. At higher temperature, the diffusion resistance in adsorbent decreases with increasing temperature, so the sorbent reached saturation quickly.

The adsorption capacities of MCF(c)/PEI-30, MCF(c)/PEI-50, MCF(c)/PEI-70, and MCF(c)/PEI-80 at different temperatures are shown in Fig. 5b. It can be seen that adsorption capacity increased with increasing temperature for each sample. When a highest adsorption capacity was obtained, it decreased as the temperature increased further. The adsorption of CO_2 over PEI-loaded adsorbent is a thermodynamically and kinetically controlled process. A series of studies have shown that temperature has a great influence on CO_2 adsorption capacity of PEI-modified support. At low temperature, CO_2 adsorption is more a

Table 1 Textural parameters of MCF materials prepared in this study

Samples	Pore volume (cm^3/g)	BET surface area (m^2/g)	Cell diameter (nm)	Window diameter (nm)
MCF(c)	2.38	557.32	20.46	16.52
MCF(a)	0.39	50.80	23.80	13.98
MCF(w_1)	0.84	94.21	32.23	18.36
MCF(w_2)	1.29	204.20	21.78	14.82
MCF(w_3)	1.45	228.19	21.78	15.15
MCF(c)/PEI-30	0.48	130.05	13.06	9.34
MCF(c)/PEI-50	0.09	19.15	17.91	11.20
MCF(c)/PEI-70	0.02	1.14	39.26	37.52
MCF(c)/PEI-80	–	0.01	–	–
MCF(c)/PEI + DETA	0.12	20.60	23.37	15.53
MCF(c)/PEI + APTMS	0.15	20.24	24.42	15.91
MCF(c)/PEI + Hep	0.17	43.53	14.01	8.58
MCF(a)/PEI-50	–	0.25	–	–
MCF(w_1)/PEI-50	0.04	3.78	70.81	61.66
MCF(w_2)/PEI-50	0.15	21.05	29.55	16.92
MCF(w_3)/PEI-50	0.26	38.25	25.74	17.33
MCF(w_2)/PEI-60	0.02	2.37	37.97	33.18
MCF(w_3)/PEI-60	0.07	7.86	33.96	21.60
MCF(w_2)/PEI-70	–	0.09	–	–
MCF(w_3)/PEI-70	–	0.58	–	–

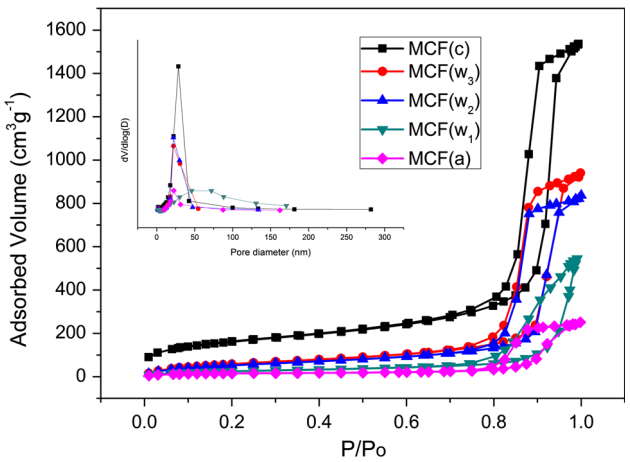

Fig. 3 Nitrogen adsorption–desorption isotherms of MCF(c), MCF(a), MCF(w_1), MCF(w_2), and MCF(w_3) at 77 k

kinetically controlled process. Though CO_2 adsorption rate is higher than desorption rate, the diffusion of CO_2 molecules into PEI bulk is the main barrier for CO_2 adsorption. At high temperature, the increase in temperature gives CO_2 molecules more energy to diffuse to the adsorption site. As a result, CO_2 adsorption capacity increases with the temperature when it is below an optimal adsorption temperature. When the temperature continues to increase, CO_2 diffusion resistance is not the main barrier and CO_2 adsorption is more a thermodynamically controlled process. The process of CO_2 adsorption is exothermic, so an increasing temperature causes a converse shift in equilibrium, and the adsorption capacity decreases.

It should be pointed out that the optimal adsorption temperature for varying PEI loading amount is different. With lower PEI loading of 30 %, the adsorbent reached the highest adsorbent capacity of 1.10 mmol/g at 65 °C. However, for adsorbent with 50 and 70 % PEI loading, the optimal adsorption temperature was 75 °C and the capacities were 1.75 and 2.95 mmol/g, respectively. When PEI loading continued to increase, the loading amount exceeded theoretical maximum amount (70.41 wt%) and the optimal temperature of CO_2 adsorption was 85 °C (2.76 mmol/g) for MCF(c)/PEI-80. CO_2 molecules should overcome more resistance to diffuse into PEI bulk in the adsorbent with higher PEI loading, which need more energy. So the optimal adsorption temperature shifts to higher value with increasing PEI loading.

The pore structure of the support is not the only factor affecting CO_2 adsorption capacity. Meanwhile, PEI loading amount and adsorption temperature work together. In order to obtain high CO_2 adsorption capacity, workers often modify mesoporous silica with high amine loading. This is

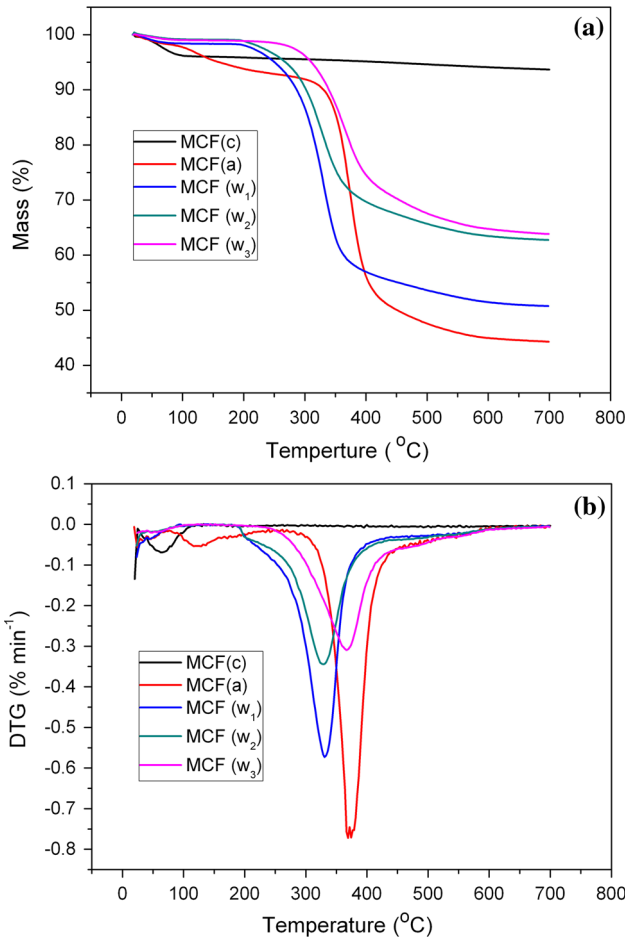

Fig. 4 **a** TGA profiles of MCF(c), MCF(a), MCF(w_1), MCF(w_2), and MCF(w_3), **b** DTGA results of MCF(c), MCF(a), MCF(w_1), MCF(w_2), and MCF(w_3)

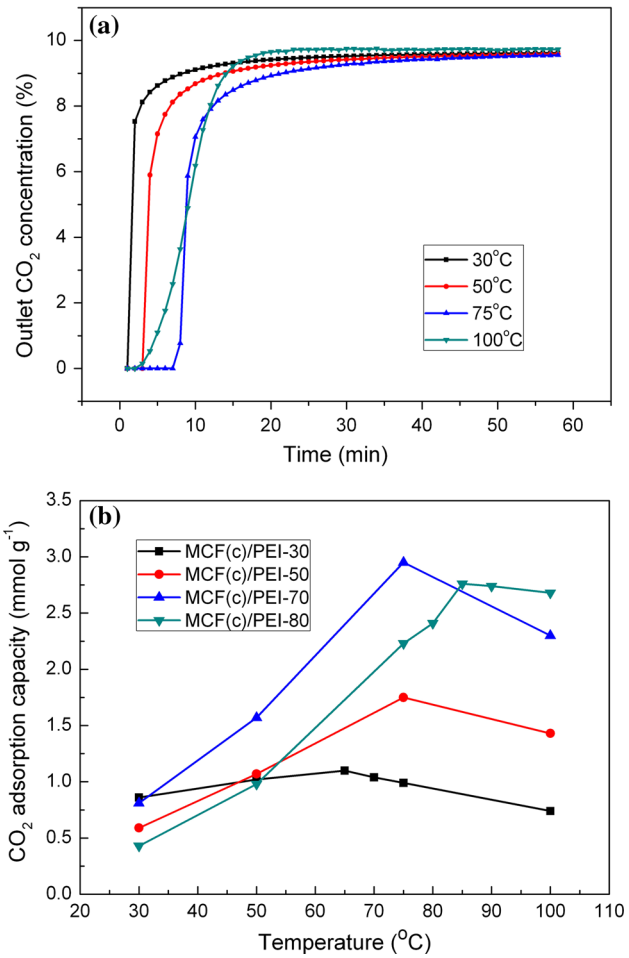

Fig. 5 **a** Breakthrough *curves* of MCF(c)/PEI-70 at different temperatures; **b** Adsorption capacity of MCF(c)/PEI-30, MCF(c)/PEI-50, MCF(c)/PEI-70 and MCF(c)/PEI-80 at different temperatures

favorable at high temperature, and an example is shown in Fig. 6a. As seen, MCF(c)/PEI-70 exhibited significantly higher and faster CO_2 uptake than MCF(c)/PEI-30 did at 75 °C. However, the diffusion resistance of CO_2 molecules also increases with increasing PEI loading, especially at low temperatures. It adversely affects the CO_2 adsorption capacity and rate, which can be seen in Fig. 6b. To circumvent the adverse effect of the diffusion limitation at low temperature, it is recommended to use adsorbents with lower PEI loading at low temperature. Under such conditions, the CO_2 adsorption will be controlled by much faster adsorption kinetics associated with the better dispersion of PEI at low content, thus diminishing the diffusion resistance. It can be seen from Fig. 6b that MCF(c)/PEI-30 adsorbed more CO_2 before breakthrough than MCF(c)/PEI-70 did. So the highest adsorption capacity (0.86 mmol/g) at 30 °C was obtained by MCF(c)/PEI-30, and the highest adsorption capacity (2.68 mmol/g) at 100 °C was obtained by MCF(c)/PEI-80.

The effect of mixed amines

Figure 7a presents the N_2 adsorption–desorption isotherms of the samples MCF(c)/PEI + DETA, MCF(c)/PEI + APTMS, MCF(c)/PEI-70, MCF(c)/PEI-50, and MCF(c)/PEI + Hep 77 K, and the corresponding adsorption pore diameter distributions are showed in inset picture. It can be seen that after modification, the pore volume and surface area decreased greatly. Comparison with MCF(c)/PEI-70, MCF(c)/PEI + DETA, and MCF(c)/PEI + APTMS exhibited higher surface area and pore volume, and the same situation occurred on sample MCF(c)/PEI + Hep and MCF(c)/PEI-50. Figure 7b shows the Fourier transform infrared spectra of mixed-amine-modified adsorbents, and the spectrum of the support is also included for comparison. The SiO_2 porous material MCF(c) show a strong peak near 1050 cm^{-1} due to the Si–O–Si asymmetric stretching, which can be seen for all the samples. After impregnation

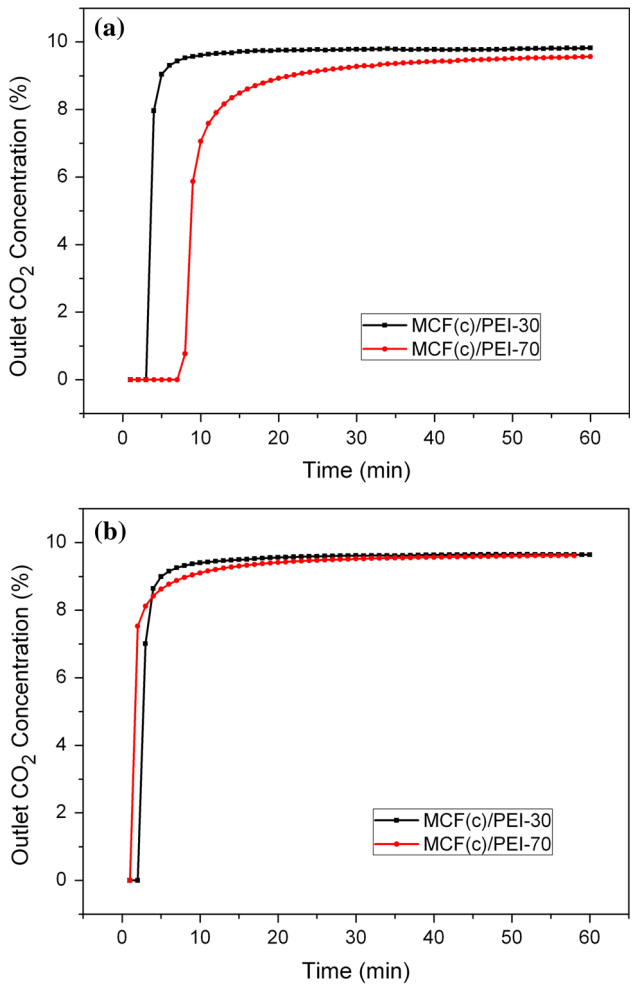

Fig. 6 **a** Breakthrough curves of MCF(c)/PEI-30 and MCF(c)/PEI-70 at 75 °C, **b** breakthrough curves of MCF(c)/PEI-30 and MCF(c)/PEI-70 at 30 °C

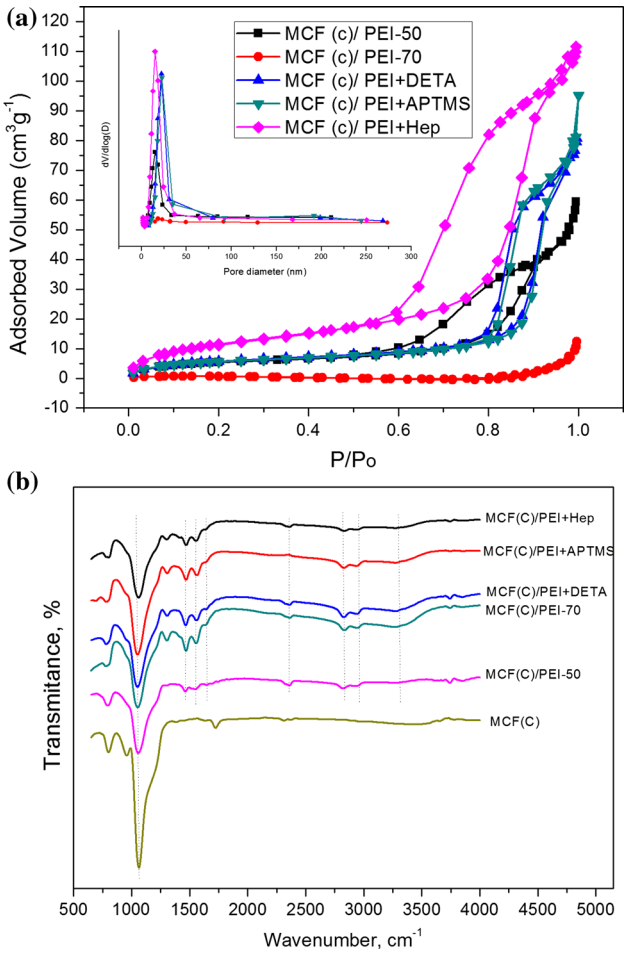

Fig. 7 **a** N_2 adsorption–desorption isotherms of the samples MCF(c)/PEI + DETA, MCF(c)/PEI + APTMS, MCF(c)/PEI-70, MCF(c)/PEI-50, and MCF(c)/PEI + Hep at 77 K and the corresponding adsorption pore diameter distributions, **b** FT-IR spectra of the samples MCF(c), MCF(c)/PEI + DETA, MCF(c)/PEI + APTMS, MCF(c)/PEI-70, MCF(c)/PEI-50, and MCF(c)/PEI + Hep

of PEI and mixed amine, weak peaks due to C–H asymmetric stretching and symmetric stretching appear near 2830 and 2940 cm^{-1}. A weak and broad peak due to N–H stretching can also be observed near 3260 cm^{-1} for all the samples. In the spectra of all the adsorbents, a peak near 1470 cm^{-1} was assigned to C–H deformation. Considering that these adsorbents are exposed to CO_2 molecules, peaks near 1660 and 1560 cm^{-1} were observed, which can be assigned to N–H deformation in RNH3+, C=O stretching due to the carbamate formed. [30] A broad peak near 2450 cm^{-1} is the result of chemically sorbed CO_2 molecules.

Figure 8 shows the CO_2 adsorption capacities for MCF(c)/PEI + DETA, MCF(c)/PEI + APTMS, and MCF(c)/PEI-70 at different temperatures. Mixed-amine-modified mesocellular silica foam MCF(c)/PEI + DETA and MCF(c)/PEI + APTMS exhibited similar CO_2 adsorption capacity of 2.99 and 2.95 mmol/g compared with that of MCF(c)/PEI-70 at 75 °C. MCF(c)/PEI + DETA exhibited higher adsorption than MCF(c)/PEI + APTMS, which could be ascribed to the more amine sites of DETA. It can be seen that MCF(c)/PEI + DETA and MCF(c)/PEI + APTMS outperformed the sample MCF(c)/PEI-70 at lower temperatures, such as 30 and 50 °C. In particular, MCF(c)/PEI + APTMS reached CO_2 adsorption capacity of 1.38 and 2.64 mmol/g at 30 and 50 °C. It is likely that mixed-amine-modified MCF(c) exhibit more amine accessibilities with larger surface area and pore volume, leading to higher adsorption capacity. In addition, the APTES or DETA mixed into PEI makes PEI better-distributed, resulting in lower diffusion resistance. This can explain why MCF(c)/PEI + APTMS presented better adsorption performance than MCF(c)/PEI + DETA, although they had similar surface area and pore volume. Sayari et al. [31] reported that alkyl chains

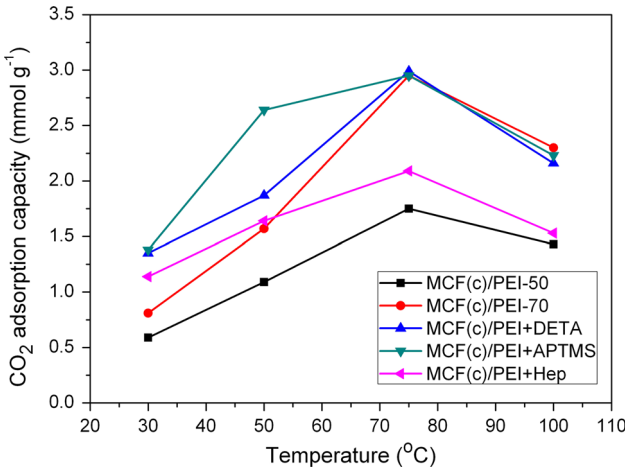

Fig. 8 Adsorption capacities of MCF(c)/PEI-50, MCF(c)/PEI-70, MCF(c)/PEI + DETA, MCF(c)/PEI + APTMS and MCF(c)/PEI + Hep at different temperatures

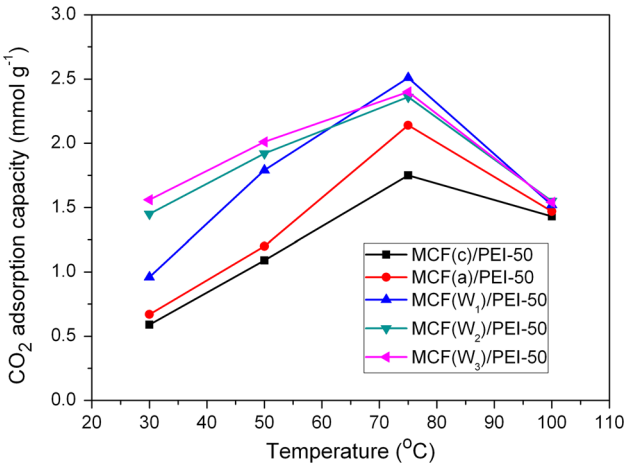

Fig. 9 Adsorption capacities of MCF(c)/PEI-50, MCF(a)/PEI-50, MCF(w1)/PEI-50, MCF(w2)/PEI-50 and MCF(w3)/PEI-50 at different temperatures

played an important role in enhancing the dispersion of PEI, thus decreasing the diffusion resistance. So MCF(c) modified by APTES with longer chains exhibited better CO_2 adsorption performance than the one modified by DETA. Compared with DETA, APTES with long alkyl chains makes more contribution to PEI dispersion, resulting in higher adsorption capacity at 30 and 50 °C. In order to demonstrate the effect of mixed amines, the *N* contents in these three samples were measured by elemental analyzer (CHN) and the amine efficiencies were calculated. The results presented that *N* contents were 18.25, 17.28, and 16.62 % for samples MCF(c)/PEI-70, MCF(c)/PEI + DETA, and MCF(c)/PEI + APTMS. And the corresponding amine efficiencies were 6.35, 10.94, and 11.63 % at 30 °C, and 12.03, 15.15, and 22.24 % at 50 °C, respectively. Sample MCF(c)/PEI + APTMS with the lowest *N* content got the highest amine efficiency at low temperatures, demonstrating the better PEI dispersion by APTMS.

In order to further demonstrate the effect of alkyl chain, a sample with 50 % PEI and 10 % heptanes was prepared in this study. It can be seen in Fig. 8 that MCF(c)/PEI + Hep showed higher adsorption capacity at all temperatures compared with MCF(c)/PEI-50. The PEI loading amount in these two samples was same, so the increased CO_2 adsorption capacity in MCF(c)/PEI + Hep was contributed to the effect of heptanes. Heptanes in the support make PEI better-distributed, resulting in lower diffusion resistance and higher adsorption capacity.

The effect of template

Figure 9 presents the CO_2 adsorption capacities for MCF(c)/PEI-50, MCF(a)/PEI-50, MCF(w_1)/PEI-50, MCF(w_2)/PEI-50, and MCF(w_3)/PEI-50 at different temperatures. It can be seen that MCF(c)/PEI-50 with no remaining template exhibited lowest CO_2 adsorption capacity,which demonstrated that remaining template was beneficial to CO_2 adsorption capacity. However, when the surfactant totally remained, the adsorption capacity of MCF(a)/PEI-50 was less than that of other three samples with lower remaining amount, which was ascribed to the low surface area and pore volume. MCF(w_1)/PEI-50 with 47.58 % template remaining exhibited lower CO_2 adsorption capacity at lower temperature. However, it reached CO_2 adsorption capacity of 2.51 mmol/g at 75 °C in these five samples, which could be attributed to the ether groups in P123 that acted as hydrogen ion receptors due to their strong H^+ affinity [26].

$$CO_2 + R'O- + R_2NH \rightarrow R'OH + - + R_2NCOO-$$

Although the CO_2 adsorption capacities of samples prepared by the supports with remaining template are higher than the one prepared by MCF(c), the CO_2 adsorption capacity does not increase with increasing amount of remaining template, which is disagreed with the conclusion made by Yan et al. [26]. This is reasonable because that the highest amount of remaining template was about 40 % in Yan's study, which is almost the same as the lowest amount of remaining template in our study. We conclude that the remaining template is not the only factor that determines CO_2 adsorption capacity, surface area, and pore volume work together.

MCF(w_3)/PEI-50 with the lowest remaining template of 35.18 % showed the highest adsorption capacity of 1.56 mmol/g at 30 °C in this study, which was about 2.64 times as high as the value of MCF(c)/PEI-50. MCF(w_3)/

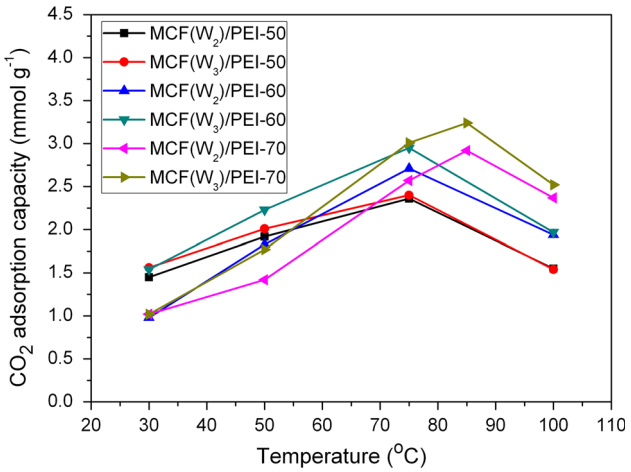

Fig. 10 CO_2 adsorption capacities for MCF(w_2) and MCF(w_3) with different PEI loadings at different temperatures

PEI-50 also showed the highest adsorption value of 2.01 mmol/g at 50 °C in these five samples. MCF(w_2)/PEI-50 with similar amount of remaining template exhibited similar CO_2 adsorption capacity of 1.45 and 1.92 mmol/g at 30 and 50 °C. The extraordinary CO_2 adsorption capacity at low temperature was attributed to the effect of template P123, which was beneficial for PEI dispersion. Also, MCF(w_3)/PEI-50 and MCF(w_2)/PEI-50 exhibited higher surface area and pore volume than MCF(w_1)/PEI-50, supplying more adsorption sites for CO_2 molecules. Considering the different performances of these samples with varying amount of remaining template at different temperatures, it can be concluded that the P123 tends to be hydrogen ion receptors at high temperature and dispersing agent at low temperature, which need further discussion.

Figure 10 shows the CO_2 adsorption capacities of MCF(w_2) and MCF(w_3) with different amounts of PEI loading at different temperatures. It presented the similar trend with that of MCF(c). The optimal adsorption temperature shifts to higher temperature with increasing PEI loading. The highest adsorption capacity was obtained by MCF(w_3)/PEI-70 at 85 °C, which is higher than the theoretical PEI loading amount. MCF(w_3)/PEI-70 exhibited higher adsorption capacities than MCF(c)/PEI-70 at all temperatures, while MCF(w_2)/PEI-70 did not. The CO_2 adsorption capacities of three samples prepared by MCF(w_3) outperformed that of samples prepared by MCF(w_2) at all temperatures. With similar remaining template amount, the higher adsorption capacity of MCF(w_3) could be ascribed to the higher pore volume and surface area. It presented that there was a synergic effect among the parameters of remaining template, surface area, and pore volume, which played a great role in CO_2 adsorption capacity.

Conclusions

The adsorption of CO_2 on calcined and water-washed MCF with different PEI loadings was investigated at different temperatures. For these two kinds of samples, the optimal adsorption temperature shifts to higher temperature with increasing PEI loading. The optimal adsorption temperature is 65 °C with low PEI loading amount of 30 %. When PEI loading exceeds the theoretical amount, the optimal temperature is 85 °C. It is demonstrated that in addition to the pore volume, pore size, and surface area, the dispersion of PEI plays an important role in the performance of CO_2 adsorption. PEI is better distributed with the help of remaining template, which is beneficial to high CO_2 adsorption capacity. Meanwhile, ether groups in template P123 contribute to CO_2 adsorption capacity by increasing the adsorption sites. Except for remaining template, mixed amine can also contributed to dispersion of PEI, especially at low temperature. Even heptanes with no amine site have the similar effect, though the contribution of heptanes is not as much as that of APTMS or DETA.

Acknowledgements This research work was financially supported by the National Natural Science Foundation of China (51272183), The Hubei Provincial Natural Science Foundation (2012FFA042), and the self-determined and innovative research funds of Wuhan University.

References

1. Liu J, Thallapally PK, McGrail BP, Brown DR, Liu J (2012) Progress in adsorption-based CO_2 capture by metal–organic frameworks. Chem Soc Rev 41(6):2308–2322
2. Remy T, Peter SA, Van Tendeloo L, Van der Perre S, Lorgouilloux Y, Kirschhock CE, Baron GV, Denayer JF (2013) Adsorption and separation of CO_2 on KFI zeolites: effect of cation type and Si/Al ratio on equilibrium and kinetic properties. Langmuir 29(16):4998–5012
3. Pham TD, Liu Q, Lobo RF (2013) Carbon dioxide and nitrogen adsorption on cation-exchanged SSZ-13 zeolites. Langmuir 29(2):832–839
4. Bae T-H, Hudson MR, Mason JA, Queen WL, Dutton JJ, Sumida K, Micklash KJ, Kaye SS, Brown CM, Long JR (2013) Evaluation of cation-exchanged zeolite adsorbents for post-combustion carbon dioxide capture. Energy Environ Sci 6(1):128–138
5. Su F, Lu C (2012) CO_2 capture from gas stream by zeolite 13X using a dual-column temperature/vacuum swing adsorption. Energy Environ Sci 5(10):9021–9027
6. Lee CS, Ong YL, Aroua MK, Daud WMAW (2013) Impregnation of palm shell-based activated carbon with sterically hindered amines for CO_2 adsorption. Chem Eng J 219:558–564
7. Shafeeyan MS, Daud WMAW, Houshmand A, Arami-Niya A (2011) Ammonia modification of activated carbon to enhance carbon dioxide adsorption: effect of pre-oxidation. Appl Surf Sci 257(9):3936–3942
8. Houshmand A, Daud WMAW, Lee M-G, Shafeeyan MS (2011) Carbon dioxide capture with amine-grafted activated carbon. Water Air Soil Poll 223(2):827–835

9. Jang D-I, Park S-J (2012) Influence of nickel oxide on carbon dioxide adsorption behaviors of activated carbons. Fuel 102:439–444
10. Wang Q, Gao Y, Luo J, Zhong Z, Borgna A, Guo Z, O'Hare D (2013) Synthesis of nano-sized spherical Mg_3Al–CO_3 layered double hydroxide as a high-temperature CO_2 adsorbent. RSC Adv 3(10):3414–3420
11. Wang Q, Tay HH, Zhong Z, Luo J, Borgna A (2012) Synthesis of high-temperature CO_2 adsorbents from organo-layered double hydroxides with markedly improved CO_2 capture capacity. Energy Environ Sci 5(6):7526–7530
12. Wang J, Stevens LA, Drage TC, Snape CE, Wood J (2012) Preparation and CO_2 adsorption of amine modified layered double hydroxide via anionic surfactant-mediated route. Chem Eng J 181–182:267–275
13. Martunus, Helwani Z, Wiheeb AD, Kim J, Othman MR (2012) Improved carbon dioxide capture using metal reinforced hydrotalcite under wet conditions. Int J Greenh Gas Control 7:127–136
14. Wang Q, Wu Z, Tay HH, Chen L, Liu Y, Chang J, Zhong Z, Luo J, Borgna A (2011) High temperature adsorption of CO_2 on Mg–Al hydrotalcite: effect of the charge compensating anions and the synthesis pH. Catal Today 164(1):198–203
15. Xu H, He Y, Zhang Z, Xiang S, Cai J, Cui Y, Yang Y, Qian G, Chen B (2013) A microporous metal–organic framework with both open metal and Lewis basic pyridyl sites for highly selective C_2H_2/CH_4 and C_2H_2/CO_2 gas separation at room temperature. J Mater Chem A 1(1):77–81
16. Nugent P, Belmabkhout Y, Burd SD, Cairns AJ, Luebke R, Forrest K, Pham T, Ma S, Space B, Wojtas L, Eddaoudi M, Zaworotko MJ (2013) Porous materials with optimal adsorption thermodynamics and kinetics for CO_2 separation. Nature 495(7439):80–84
17. Yang D-A, Cho H-Y, Kim J, Yang S-T, Ahn W-S (2012) CO_2 capture and conversion using Mg-MOF-74 prepared by a sonochemical method. Energy Environ Sci 5(4):6465–6473
18. Wang X, Ma X, Song C, Locke DR, Siefert S, Winans RE, Möllmer J, Lange M, Möller A, Gläser R (2013) Molecular basket sorbents polyethylenimine–SBA-15 for CO_2 capture from flue gas: characterization and sorption properties. Microporous Mesoporous Mater 169:103–111
19. Olea A, Sanz-Pérez ES, Arencibia A, Sanz R, Calleja G (2013) Amino-functionalized pore-expanded SBA-15 for CO_2 adsorption. Adsorption 19(2–4):589–600
20. Wang X, Ma X, Schwartz V, Clark JC, Overbury SH, Zhao S, Xu X, Song C (2012) A solid molecular basket sorbent for CO_2 capture from gas streams with low CO_2 concentration under ambient conditions. Phys Chem Chem Phys 14(4):1485–1492
21. Yan X, Zhang L, Zhang Y, Yang G, Yan Z (2011) Amine-Modified SBA-15: effect of pore structure on the performance for CO_2 capture. Ind Eng Chem Res 50(6):3220–3226
22. Heydari-Gorji A, Yang Y, Sayari A (2011) Effect of the pore length on CO_2 adsorption over amine-modified mesoporous silicas. Energy Fuel 25(9):4206–4210
23. Ma X, Wang X, Song C (2009) "Molecular Basket" sorbents for separation of CO_2 and H_2S from various gas streams. J Am Chem Soc 131(16):5777–5783
24. Son W-J, Choi J-S, Ahn W-S (2008) Adsorptive removal of carbon dioxide using polyethyleneimine-loaded mesoporous silica materials. Microporous Mesoporous Mater 113(1–3):31–40
25. Zhao J, Simeon F, Wang Y, Luo G, Hatton TA (2012) Polyethylenimine-impregnated siliceous mesocellular foam particles as high capacity CO_2 adsorbents. RSC Adv 2(16):6509–6519
26. Yan W, Tang J, Bian Z, Hu J, Liu H (2012) Carbon dioxide capture by amine-impregnated mesocellular-foam-containing template. Ind Eng Chem Res 51(9):3653–3662
27. Yan X, Zhang L, Zhang Y, Qiao K, Yan Z, Komarneni S (2011) Amine-modified mesocellular silica foams for CO_2 capture. Chem Eng J 168(2):918–924
28. Subagyono DJN, Liang Z, Knowles GP, Chaffee AL (2011) Amine modified mesocellular siliceous foam (MCF) as a sorbent for CO_2. Chem Eng Res Des 89(9):1647–1657
29. Qi G, Fu L, Choi BH, Giannelis EP (2012) Efficient CO_2 sorbents based on silica foam with ultra-large mesopores. Energy Environ Sci 5(6):7368–7375
30. Qi G, Wang Y, Estevez L, Duan X, Anako N, Park A-HA, Li W, Jones CW, Giannelis EP (2011) High efficiency nanocomposite sorbents for CO_2 capture based on amine-functionalized mesoporous capsules. Energy Environ Sci 4(2):444–452
31. Heydari-Gorji A, Belmabkhout Y, Sayari A (2011) Polyethylenimine-impregnated mesoporous silica: effect of amine loading and surface alkyl chains on CO_2 adsorption. Langmuir 27(20):12411–12416
32. Chen C, Son W-J, You K-S, Ahn J-W, Ahn W-S (2010) Carbon dioxide capture using amine-impregnated HMS having textural mesoporosity. Chem Eng J 161(1–2):46–52
33. Stuckert NR, Yang RT (2011) CO_2 capture from the atmosphere and simultaneous concentration using zeolites and amine-grafted SBA-15. Environ Sci Technol 45(23):10257–10264
34. Zukal A, Jagiello J, Mayerova J, Cejka J (2011) Thermodynamics of CO_2 adsorption on functionalized SBA-15 silica. NLDFT analysis of surface energetic heterogeneity. Phys Chem Chem Phys 13(34):15468–15475
35. Bollini P, Brunelli NA, Didas SA, Jones CW (2012) Dynamics of CO_2 adsorption on amine adsorbents. 1. Impact of heat effects. Ind Eng Chem Res 51(46):15145–15152
36. Yao M, Dong Y, Feng X, Hu X, Jia A, Xie G, Hu G, Lu J, Luo M, Fan M (2014) The effect of post-processing conditions on aminosilane functionalizaiton of mesocellular silica foam for post-combustion CO_2 capture. Fuel 123:66–72
37. Oh S, Kang T, Kim H, Moon J, Hong S, Yi J (2007) Preparation of novel ceramic membranes modified by mesoporous silica with 3-aminopropyltriethoxysilane (APTES) and its application to Cu2 + separation in the aqueous phase. J Membr Sci 301(1–2):118–125
38. Cui S, Cheng W, Shen X, Fan M, Russell A, Wu Z, Yi X (2011) Mesoporous amine-modified SiO_2 aerogel: a potential CO_2 sorbent. Energy Environ Sci 4(6):2070–2074
39. Hiyoshi N, Yogo K, Yashima T (2005) Adsorption characteristics of carbon dioxide on organically functionalized SBA-15. Microporous Mesoporous Mater 84(1–3):357–365
40. Li Y, Sun N, Li L, Zhao N, Xiao F, Wei W, Sun Y, Huang W (2013) Grafting of amines on ethanol-extracted SBA-15 for CO_2 adsorption. Materials 6(3):981–999
41. Knöfel C, Descarpentries J, Benzaouia A, Zeleňák V, Mornet S, Llewellyn PL, Hornebecq V (2007) Functionalised micro-/mesoporous silica for the adsorption of carbon dioxide. Microporous Mesoporous Mater 99(1–2):79–85
42. Wei J, Shi J, Pan H, Zhao W, Ye Q, Shi Y (2008) Adsorption of carbon dioxide on organically functionalized SBA-16. Microporous Mesoporous Mater 116(1–3):394–399
43. Sanz R, Calleja G, Arencibia A, Sanz-Pérez ES (2013) Development of high efficiency adsorbents for CO_2 capture based on a double-functionalization method of grafting and impregnation. J Mater Chem A 1(6):1956–1962
44. Calleja G, Sanz R, Arencibia A, Sanz-Pérez ES (2011) Influence of drying conditions on amine-functionalized SBA-15 as adsorbent of CO_2. Top Catal 54(1–4):135–145
45. Zeleňák V, Badaničová M, Halamová D, Čejka J, Zukal A, Murafa N, Goerigk G (2008) Amine-modified ordered mesoporous silica: effect of pore size on carbon dioxide capture. Chem Eng J 144(2):336–342

46. Chang F-Y, Chao K-J, Cheng H-H, Tan C-S (2009) Adsorption of CO_2 onto amine-grafted mesoporous silicas. Sep Purif Technol 70(1):87–95
47. Young PD, Notestein JM (2011) The role of amine surface density in carbon dioxide adsorption on functionalized mixed oxide surfaces. ChemSusChem 4(11):1671–1678
48. Bacsik Z, Ahlsten N, Ziadi A, Zhao G, Garcia-Bennett AE, Martin-Matute B, Hedin N (2011) Mechanisms and kinetics for sorption of CO_2 on bicontinuous mesoporous silica modified with n-propylamine. Langmuir 27(17):11118–11128
49. Lu C, Su F, Hsu S-C, Chen W, Bai H, Hwang JF, Lee H-H (2009) Thermodynamics and regeneration of CO_2 adsorption on mesoporous spherical-silica particles. Fuel Process Technol 90(12):1543–1549
50. Serna-Guerrero R, Belmabkhout Y, Sayari A (2010) Triamine-grafted pore-expanded mesoporous silica for CO_2 capture: effect of moisture and adsorbent regeneration strategies. Adsorption 16(6):567–575
51. Kim S, Ida J, Guliants VV, Lin JYS (2005) Tailoring pore properties of MCM-48 silica for selective adsorption of CO_2. J Phys Chem B 109(13):6287–6293
52. Wang X, Li H, Liu H, Hou X (2011) AS-synthesized mesoporous silica MSU-1 modified with tetraethylenepentamine for CO_2 adsorption. Microporous Mesoporous Mater 142(2–3):564–569
53. Zhao W, Zhang Z, Li Z, Cai N (2013) Investigation of thermal stability and continuous CO_2 capture from flue gases with supported amine sorbent. Ind Eng Chem Res 52(5):2084–2093
54. Zhang Z, Ma X, Wang D, Song C, Wang Y (2012) Development of silica–gel-supported polyethylenimine sorbents for CO_2 capture from flue gas. AIChE J 58(8):2495–2502
55. Li W, Bollini P, Didas SA, Choi S, Drese JH, Jones CW (2010) Structural changes of silica mesocellular foam supported amine-functionalized CO_2 adsorbents upon exposure to steam. ACS Appl Mater Interfaces 2(11):3363–3372
56. Feng X, Hu G, Hu X, Xie G, Xie Y, Lu J, Luo M (2013) Tetraethylenepentamine-modified siliceous mesocellular foam (MCF) for CO_2 capture. Ind Eng Chem Res 52(11):4221–4228
57. Yue MB, Sun LB, Cao Y, Wang ZJ, Wang Y, Yu Q, Zhu JH (2008) Promoting the CO_2 adsorption in the amine-containing SBA-15 by hydroxyl group. Microporous Mesoporous Mater 114(1–3):74–81
58. Yue MB, Sun LB, Cao Y, Wang Y, Wang ZJ, Zhu JH (2008) Efficient CO_2 capturer derived from as-synthesized MCM-41 modified with amine. Chemistry 14(11):3442–3451
59. Yue MB, Chun Y, Cao Y, Dong X, Zhu JH (2006) CO_2 capture by as-prepared SBA-15 with an occluded organic template. Adv Funct Mater 16(13):1717–1722
60. Wang J, Long D, Zhou H, Chen Q, Liu X, Ling L (2012) Surfactant promoted solid amine sorbents for CO_2 capture. Energy Environ Sci 5(2):5742–5749
61. Fauth DJ, Gray ML, Pennline HW, Krutka HM, Sjostrom S, Ault AM (2012) Investigation of porous silica supported mixed-amine sorbents for post-combustion CO_2 capture. Energy Fuel 26(4):2483–2496
62. Sun JM, Zhang H, Ma D, Chen YY, Bao XH, Klein-Hoffmann A, Pfander N, Su DS (2005) Alkanes-assisted low temperature formation of highly ordered SBA-15 with large cylindrical mesopores. Chem Commun 42:5343–5345
63. Wang XX, Schwartz V, Clark JC, Ma XL, Overbury SH, Xu XC, Song CS (2009) Infrared study of CO_2 sorption over "Molecular Basket" sorbent consisting of polyethylenimine-modified mesoporous molecular sieve. J Phys Chem C 113(17):7260–7268